nature geoscience

LETTERS

PUBLISHED ONLINE: XX MONTH XXXX | DOI: 10.1038/NGEO1356

Impact of transient groundwater storage on the discharge of Himalayan rivers

Christoff Andermann[1,2]*, Laurent Longuevergne[1], Stéphane Bonnet[3], Alain Crave[1], Philippe Davy[1] and Richard Gloaguen[2]

In the course of the transfer of precipitation into rivers, water is temporarily stored in reservoirs with different residence times[1,2] such as soils, groundwater, snow and glaciers. In the central Himalaya, the water budget is thought to be primarily controlled by monsoon rainfall, snow and glacier melt[3,4], and secondarily by evapotranspiration[3]. An additional contribution from deep groundwater[5–7] has been deduced from the chemistry of Himalayan rivers[6], but its importance in the annual water budget remains to be evaluated. Here we analyse records of daily precipitation and discharge within significant catchments in Nepal over about 30 years. We observe annual hysteresis loops—that is, a phase shift between precipitation and discharge—in both glaciated and unglaciated catchments and independent of the geological setting. We infer that water is stored temporarily in a reservoir with characteristic response time of about 45 days, suggesting a diffusivity typical of fractured basement aquifers[8]. We estimate this transient storage capacity at about 28 km^3 for the three main Nepal catchments; snow and glacier melt contribute about 14 km^3 yr^{-1}, about 10% of the annual river discharge. We conclude that groundwater storage in a fractured basement contributes significantly to the Himalayan river discharge cycle.

The discharge of the central Himalayan rivers is governed by a strong precipitation seasonality[3,6,9,10] (Fig. 1) with up to 80% of the annual rainfall occurring during the Indian Summer Monsoon (ISM) season[3]. The ISM precipitation is the main source for glacier mass accumulation[9] and its spatial distribution is strongly influenced by orographic effects[3]. Variations in intensity and duration of the ISM, linked to El Nino/Southern Oscillation (ENSO; ref. 11), enhance the annual amount of precipitation by ~25–50% with respect to the annual mean at low to moderate elevation (>3 km), and up to 200% at high elevation[12]. Snow melt contributes to a significant fraction of river discharge in the western and eastern Himalayas and on the Tibetan plateau[3,13], but only to a minor fraction (~10%) in the central Himalayas, mainly in the early ISM (May–July)[3]. It has been suggested that rainfall-derived discharge, ice and snow melt are the primary factors controlling Himalayan river discharge, with evapotranspiration forming a secondary minor component[3]. Notwithstanding, this hydrological budget model neglects transient water storage in soils, floodplains and groundwater. However, geochemical data indicate that a non-negligible part of surface runoff originates from deep groundwater reservoirs[6].

We investigate the transfer of water within the main catchments of the Nepal Himalayas (Fig. 1a) using a daily meteorological and hydrological dataset spanning ~30 years (Table 1). We consider the three main catchments of Nepal (Sapta Koshi, Narayani and Karnali basins), some of their tributaries, and three unglaciated small catchments at the front of the Himalayan range (Fig. 1a and Table 1). The main catchments drain the entire Himalayan range of Nepal, from the Tibetan Plateau to the Lesser Himalayas. Most of their headwaters are located on the arid Plateau (Fig. 1a), characterized by a weaker influence of the ISM. The rivers incise bedrock comprising, from north to south, the low-grade Paleozoic–Mesozoic Tethyan Sediment Series, high-grade metamorphic gneisses and migmatites of the High Himalayan Crystalline series and low-grade Proterozoic sediments of the Lesser Himalayas (Fig. 1c). Most of the data considered here come from outlet stations located to the north of the Siwalik foreland. The annual specific discharge of the studied basins is typically on the order of ~10^3 mm yr^{-1} (Table 1) and their annual hydrograph clearly shows the seasonal impact of the ISM on river discharge, generally peaking in July/August[3,14] (Fig. 1b). Mean annual basin precipitation is 920, 1,396 and 920 mm yr^{-1} in the Sapta Koshi, Narayani and Karnali catchments, respectively. However, precipitation is spatially heterogeneous (Fig. 1a) and is strongly controlled by orography, reaching a maximum between elevations of 2–3 km (refs 15,16). The upper parts of the catchments are glaciated (Fig. 1a), covering between 4 and 15% of the catchment area (Table 1).

We calculated mean basin-wide daily precipitation rate and use daily discharge measurements to compute specific water discharge for all the studied drainage basins (see Methods). Plots of daily precipitation versus specific discharge highlight a considerable scatter within the ~30-year dataset (Fig. 2a). However, the chronology of the data exhibits a well-defined annual cycle, showing an increase of discharge with increasing precipitation during the pre-ISM (March–May) to the ISM (June–September) and a decrease during the post-ISM (October–November). The systematic higher discharge for a given precipitation rate during the post-ISM compared with the pre-ISM is striking. The data consequently shows an annual anticlockwise hysteresis loop (Fig. 2a). A 30-day moving average highlights the temporal consistency of the loop from year to year (Fig. 2a, inset). Data scattering results from inter-annual variability, particularly during the post-ISM, as illustrated by comparing the data during a strong or a weak ISM year (see Supplementary Fig. S1). The annual anticlockwise hysteresis loop is observed in all studied basins (Fig. 2b), regardless of the geological units, the presence of glaciers or snow cover (Table 1).

Anticlockwise hysteresis loops imply that precipitation is temporarily stored within the catchments and not transferred directly to the river during the pre-ISM and ISM seasons, whereas

[1]Géosciences Rennes, Université de Rennes 1, CNRS, Campus de Beaulieu, 35042 Rennes, France, [2]Remote Sensing Group, Geology Institute, TU Bergakademie Freiberg, B.-von-Cotta-Str. 2, 09599 Freiberg, Germany, [3]Géosciences Environnement Toulouse, Université de Toulouse, CNRS-UPS-IRD, Observatoire Midi-Pyrénées, 14 Av. Edouard Belin, 31400 Toulouse, France. *e-mail: christoff.andermann@univ-rennes1.fr.

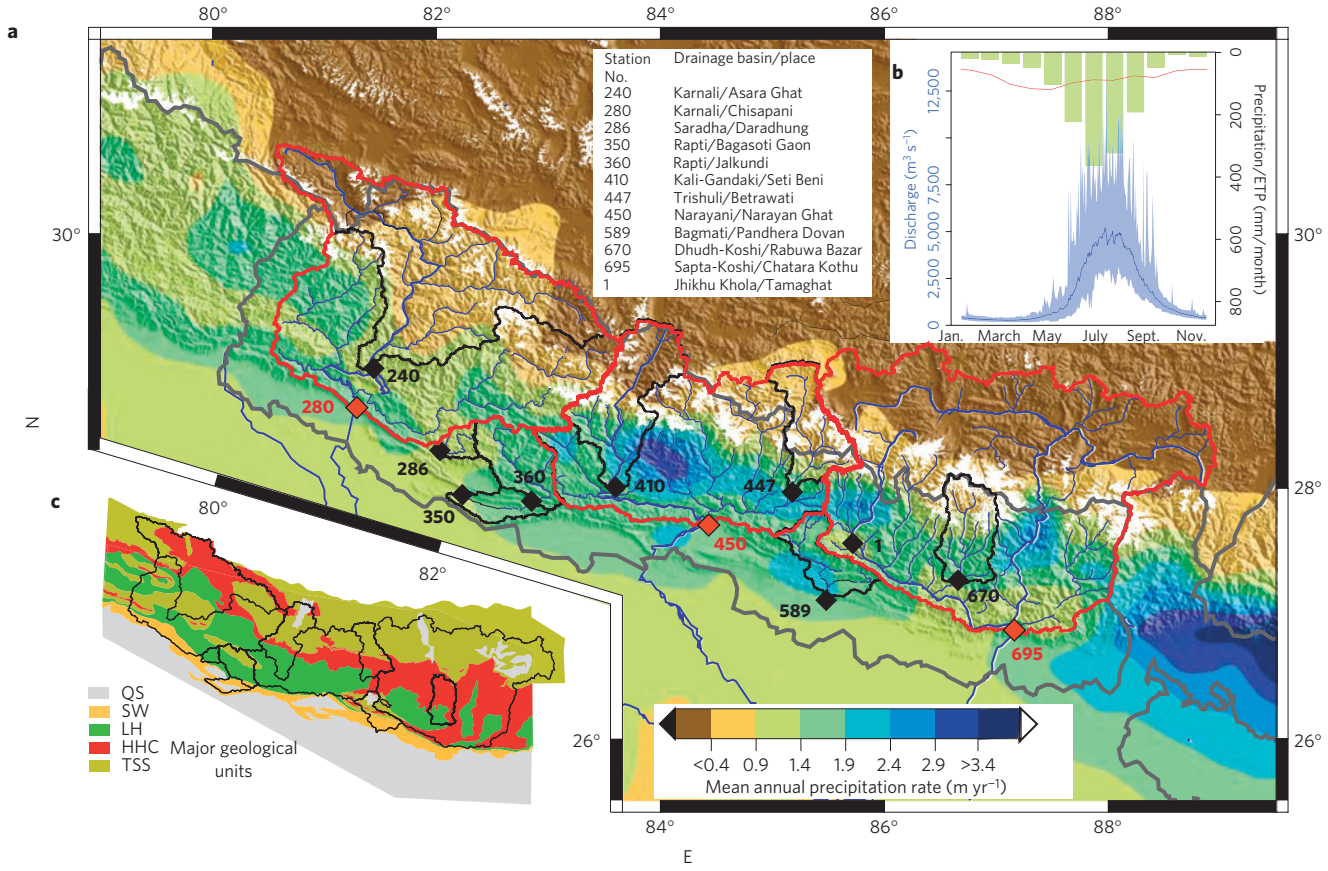

Figure 1 | Hydrological setting of the Nepal Himalayas. a, Precipitation distribution map, hydrological discharge stations used in this study (black diamonds) and contours (red lines) of the studied drainage basins. Grey lines mark political boundaries. Mean annual precipitation rates (see Methods), representing 50 years of data, are draped over shaded relief. River network is shown in blue and glaciers in white (after ref. 29). **b**, Mean basin-wide precipitation (1951–2006, in green) and potential evapotranspiration (red) for the Narayani drainage basin. The bold blue line with blue shading represents the mean, maximum and minimum daily discharge over 34 years (station 450). **c**, Simplified geological map of Nepal[30]: QS: Quaternary Sediments, SW: Siwaliks Formation, LH: metasediments of the Lesser Himalayas, HHC: High Himalayan Crystalline, TSS: Tethyan Sediment Series.

the storage compartment is drained during the post-ISM. Glaciers can be directly ruled out as the main contributor to the observed hysteresis effect because the release of water by glacier or snow melt occurs principally during the pre-ISM to ISM season[3,13] (Fig. 3b and Supplementary Fig. S2), which is not consistent with the anticlockwise nature of the hysteresis. Moreover, hysteresis effects are observed in both glaciated and unglaciated catchments (Fig. 2b). As the potential evapotranspiration in the Himalayas reaches a maximum during the pre-ISM, in April–May[17] (Fig. 1b), this could qualitatively explain the anticlockwise hysteresis loop. However, it is estimated to account for less than 10% of the overall hydrological budget[3], so this effect probably plays a minor role, mainly because the magnitude of evapotranspiration rapidly decreases with elevation[17]. Consequently, the main mechanism explaining the hysteresis effect is probably a transient storage of water in a groundwater unit during the rising ISM and its post-ISM release.

To more precisely determine the role of groundwater storage on the Himalayan hydrological cycle, we solved the water balance at catchment scale to discriminate time response distribution in discharge data and relate it to storage compartments through hydrological modelling. We used a modified version of the conceptual hydrological model GR2M (see Methods), which addresses several physical processes in a simplified, but proven robust, way in a wide range of climatological settings[18]. Because the observed hysteresis effect is a seasonal process, daily modelling of hydrological processes is not the pertinent scale for our purpose (see ref. 19). The great diversity of the involved processes, within a wide range of environmental settings, limits the reliability of short-term modelling, so we modelled the data at a monthly rather than at a daily scale. Note that we nevertheless tested daily-scale modelling (see Methods and Supplementary Table S1). Modelled daily results are generally similar to monthly ones (Table 1), but the efficiency, however, is less well described (Table 1 and Supplementary Table S1). The model simulates the catchment response to rainfall in terms of river discharge and incorporates three components (see Supplementary Fig. S3): (1) a snow module based on the HBV approach[20] (see Methods), (2) a fast rain-to-discharge flow related to quick runoff processes, and (3) a slow-flow component representing groundwater contribution. This third reservoir retards the rain-discharge response and yields baseflow during dry periods. It is characterized by a response time t_c, defined as the time for a hydrological system to reach equilibrium after the hydraulic head has changed[1]. The model is forced by precipitation, temperature and potential evapotranspiration (see Methods). We calibrated on the logarithm of all the observed daily water discharge to account for the large range of discharges, that is to apply identical weights to both high- and low-water stages, and under the constraint that total observed and modelled discharge volumes are identical. The modelling is robust in most catchments: hysteresis loops are confidently reproduced for all catchments (for example Supplementary Fig. S4) with Nash–Sutcliffe coefficients of 0.89, 0.91 and 0.92 for Sapta Koshi, Narayani and Karnali basins, respectively (Table 1). The modelling implies a significant storage of water within the slow-flow reservoir, with calculated t_c longer

Table 1 | Properties of the studied drainage basins and summary of results (monthly modelling).

Station no. Basin	240 Karnali	**280 Karnali**	286 Saradha	350 Rapti	360 Rapti	410 Kali Gandaki	447 Trishuli	**450 Narayani**	670 Dudh Koshi	**695 Sapta Koshi**	589 Bagmati	1 Jhikhu Khola
Lat (°) N	28.95	**28.64**	28.64	27.90	27.95	28.01	27.97	**27.71**	27.27	**26.87**	27.11	27.59
Long (°) E	81.44	**81.29**	82.03	82.85	82.23	83.60	85.18	**84.43**	86.66	87.16	85.48	85.67
Size (km^2)	21,121	**45,967**	808	3,648	5,198	7,169	4,428	**32,002**	3,880	**57,719**	2,849	111
Precipitation ($mm\,yr^{-1}$)	558	**920**	1,107	1,522	1,470	1,030	692	**1,396**	1,295	920	1,932	1,285
Discharge ($mm\,yr^{-1}$)	650	**789**	460	903	787	1,145	1,513	**1,145**	1,598	**1,039**	1,205	374
ETR ($mm\,yr^{-1}$)	176	**234**	656	720	654	178	121	**367**	178	**179**	839	171
Availability of discharge	1975–2006	**1973–2006**	1976–2006	1978–2006	1985–2006	1979–1995	1977–2006	**1973–2006**	1987–2006	**1977–2006**	2001–2006	1998–2006
% Area glaciated	5.9	**4.7**	0.0	0.0	0.0	10.3	6.5	**9.9**	14.7	**7.3**	0.0	0.0
Max elevation (m asl.)	7,549	**7,697**	2,800	3,623	3,623	8,147	7,352	**8,147**	8,848	**8,848**	2,795	2,200
Nash–Sutcliffe coef.	0.93	**0.92**	0.79	0.88	0.95	0.91	0.79	**0.91**	0.94	**0.89**	0.88	0.29
Recession exp. b ($Q = aS^b$)*	1.01	**1.11**	1.16	1.01	1.18	1.01	1.02	**1.16**	1.17	**1.01**	1.12	1.18
Storage capacity (km^3)	3.1±1.2	**8.1±3.3**	0.21±0.08	1.6±0.7	1.8±0.8	1.3±0.6	0.9±0.4	**9.9±3**	1.2±0.4	**10.3±6**	1.2±0.5	0.03±0.01
Storage capacity (mm)	150±60	**175±70**	260±90	430±180	350±150	180±80	200±80	**310±125**	300±105	**180±100**	440±180	300±120
t_c GR2M (days)*	46±5	**50±5**	37±3	36±8	41±8	45±4	38±4	**50±5**	53±11	**47±4**	30±5	120±35
t_c recession curve (days)*	40±10	**46±15**	37±13	44±17	42±15	41±15	44±11	**40±13**	45±9	**41 ±11**	41±19	77±24
Ice+snow melt ($km^3\,yr^{-1}$)	1.2	**4.1**	n.a.	n.a.	n.a.	0.7	0.8	**5.3**	0.6	**4.1**	n.a.	n.a.
% snow melt	12	**7**	n.a.	n.a.	n.a.	3	13	**2**	6	**5**	n.a.	n.a.
Geology units % coverage QS/SW/LH/HHC/TSS	0/0/17/44/39	**0/5/33/25/37**	0/3/96/0/1	0/5/62/0/33	8/24/45/0/23	10/0/32/15/43	0/0/8/37/55	**2/0/42/23/33**	0/0/26/73/1	**6/0/16/40/38**	13/42/2/11/32	0/0/11/17/72

Maximum elevation is used as a proxy for snow occurrence during winter (considering winter snowline at ~3,000 m asl.; ref. 16). Precipitation rate is computed as a mean basin value. Specific discharge is computed from daily river gauge data. Real evapotranspiration (ETR) is computed from our modelling (see Methods). Storage represents the mean annual amplitude of storage variation and its respective uncertainty in km^3 and mm respectively (Supplementary Fig. S2). t_c is the characteristic basin response time, derived from hydrological modelling or from the recession curve of hydrographs (see Methods). The % glaciated values are calculated using data from ref. 29. Ice melt is the annual volumetric glacier ice melt contribution to the rivers, estimated from the relative baseflow shift in the precipitation–discharge plot (Fig. 2b). % snow melt is the contribution of snow to discharge (both directly and via the aquifer). QS: Quaternary Sediments, SW: Siwaliks Formation, LH: metasediments of the Lesser Himalayas, HHC: High Himalayan Crystalline, TSS: Tethyan Sediment Series. *See Methods.

than one month (Table 1). Modelled data are in agreement with t_c values derived directly from the fit of baseflow recession curves[21] (see Methods and Table 1). This delay between precipitation and discharge yields baseflow during dry periods and is responsible for the existence of the hysteresis loops. Shorter t_c, associated with a low storage capacity (for example ten days, equivalent to twenty times smaller storage capacity), do not allow one to reproduce the observed hysteresis loops analytically (see Methods and Supplementary Fig. S5c).

The nature of the groundwater system controlling the hysteresis effect is provided by its response time t_c. For groundwater systems, t_c is inversely proportional to the hydraulic diffusivity D (transmissivity divided by storage coefficient) and is proportional to the square of the characteristic aquifer scale L_c: $t_c \sim L_c^2 D^{-1}$ (ref. 1). L_c is the characteristic distance between the aquifer and streams, which is approximately the hillslope length if aquifers are spread homogeneously over the drainage basin. Considering L_c in the range 0.5–5 km and t_c of ~45 days, equivalent diffusivity

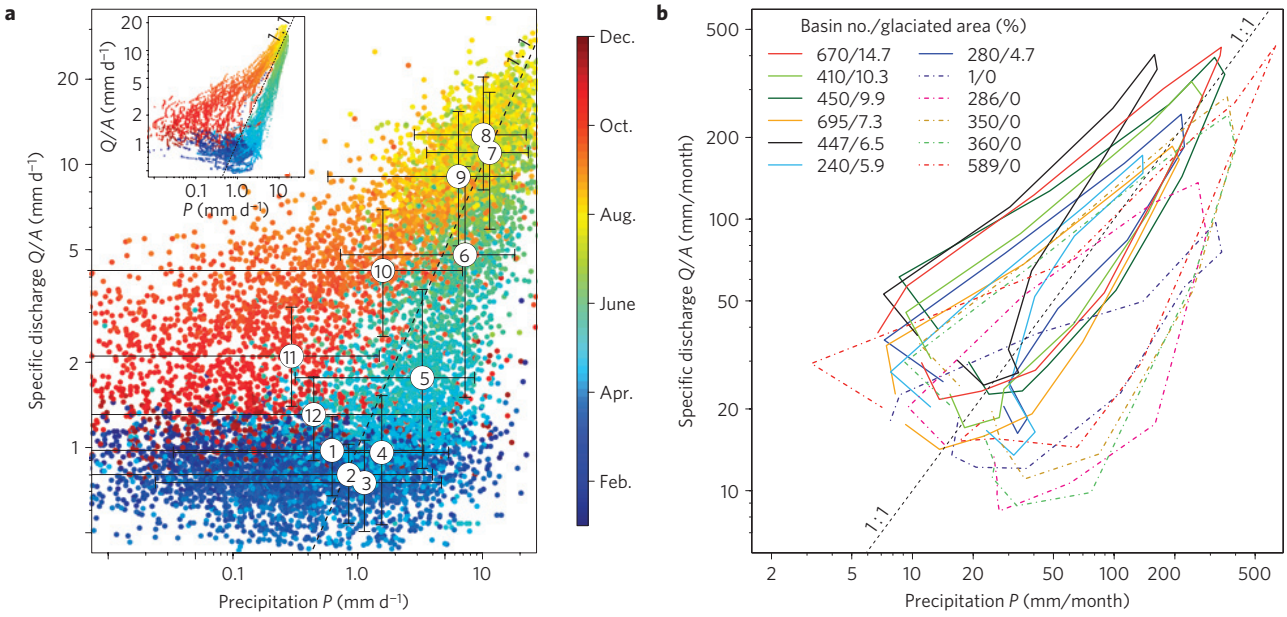

Figure 2 | Precipitation–discharge (*P*–*Q*) anticlockwise hysteresis plot. a, Bi-logarithmic *P*–*Q* plot of daily data for the Narayani basin over 34 years at station 450 (~12,300 data points). Data plotted are specific discharges (discharges normalized by drainage area) and mean basin precipitation rates. Note that discharge is not plotted when precipitation is zero. Colour bar is scaled for a calendar year. White filled circles represent the mean monthly values over 34 years, the months being indicated by numbers. The error bars represent the 5% and 95% quantiles of the daily data distribution of each month. Inset shows the data filtered with a 30-day moving average. **b**, Mean annual hysteresis loops plotted from monthly mean data for all the drainage basins. Solid lines represent partially glaciated basins and dashed lines unglaciated ones (percentage of glacial coverage from ref. 29).

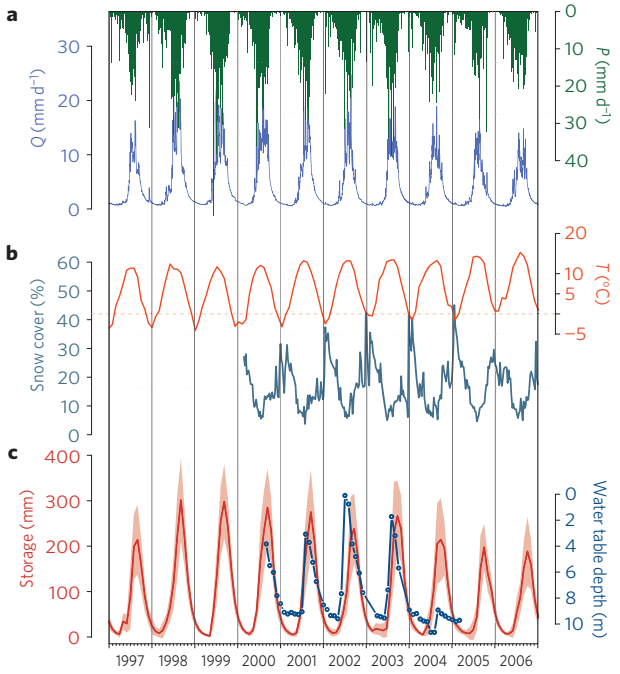

Figure 3 | 10-year (1997–2006) temporal variability of several hydrological compartments, Narayani basin. a, Daily precipitation (green) and daily specific river discharge (blue). **b**, Temperature (orange) as a glacier melt proxy (from CRU; ref. 26) and percentage of basin-wide snow cover (dark green, data from MODIS MOD10C2 v.5 (ref. 25) with an 8-day temporal resolution). **c**, Calculated groundwater storage (red), shading illustrating model uncertainty (Supplementary Fig. S2). Ground water table variation (dark blue) observed in a dug-well in Jhikhu Khola Basin[22] (station no. 1) from ref. 22 and unpublished data provided by these authors. The abnormal low water table in 2004 probably results from exhaustive exploitation.

values are about ~1 $m^2 s^{-1}$, a typical value for aquifers in fractured rocks[8] (0.01–10 $m^2 s^{-1}$). Recession curve exponents calculated on the falling limb of the post-ISM hydrograph (see Methods) are close to 1, and suggest the contribution of a confined aquifer to discharge[21]. The estimated aquifer storage capacity is ~180 mm per unit area, representing ~28 km^3 for the three main catchments of Nepal (Table 1). Modelling also indicates that the annual volume of water flowing through this groundwater system represents ~2/3 of the annual river discharge (Supplementary Table S1). The modelled storage dynamics matches the groundwater table variations observed in dug-wells, for example in Jhikhu Khola catchment[22] (Fig. 3c). The ratio between calculated water storage variations (Table 1) and water-table depth observed here indicates low porosity values of a few per cent. We conclude from low porosity values[23], confined behaviour[21] and characteristic diffusivity values[8], that the aquifer is predominantly fractured basement. Average water-table variation (total annual storage capacity divided by rock porosity, considering low porosity value) is estimated to a few tens of metres in the studied catchments.

We show that the very specific climatic regime of Nepal, characterized by distinct long-lasting wet and dry seasons and a major increase of precipitation during the ISM (Figs 1b and 3a), is responsible for the recharge of fractured basement aquifers. The aquifers are refilled during the ISM and purged in the post-ISM, leading to the annual hysteresis effect that we observed. This behaviour is observed in all the studied drainage basins, independent of their size, physiographic location or main basement geology (Fig. 1, Table 1 and Supplementary Fig. S6). Very little is known in Nepal about the actual aquifer, its physical properties and the relationship with tectonic structures. These appear as critical unknowns to go further into our understanding of deep groundwater influence on the Himalayan hydrological cycle, including water resources and flood hazard as well as on landslide risk due to pore-pressure saturation processes. Finally, it is noticeable that during winter (December–February) the precipitation–discharge graphs (Fig. 2b) show a systematic higher

baseflow for glaciated catchments compared with unglaciated ones. Because glaciers represent an additional water storage component in some catchments, this vertical shift of the hysteresis loops of glaciated catchments reveals the contribution of glacial melt (and snow in spring) to river discharge and can be used to quantify it. From this approach (see Methods), the snow and glacier melt contribution to river discharge is estimated to be $\sim 14 \pm 7\,km^3\,yr^{-1}$ considering the three main catchments in Nepal (Table 1), which accounts for ~10% of annual river discharge. In Nepal, the volume of water flowing through fractured basement aquifer is approximately six times higher than the contribution of glacial and snow melt to river discharge.

Methods

Data and data processing. Precipitation is calculated using APHRODITE (Asian Precipitation Highly Resolved Observational Data Integration Towards Evaluation of Water Resources) data (http://www.chikyu.ac.jp/precip/). Here, we use the daily version for monsoon Asia APHRO_MA_V1003R1, with a spatial resolution of 0.25° (ref. 24). It is currently the best available dataset for Nepal[10]. We use raw river discharge data provided by the Department of Hydrology and Meteorology of Nepal (DHM; see for example ref. 14), derived from daily stage readings and calibrated rating curves (no interpolated data are used). Potential evapotranspiration is estimated using an elevation-based model developed for Nepal[17]. Basin-wide snow cover is obtained from MOD10C2 version 5 (http://nsidc.org/data/mod10c2v5.html), with an 8-day temporal and 500 m spatial resolution[25]. We used the monthly temperature dataset CRU TS3.0 (ref. 26), with 0.5° gridded resolution. Daily temperature is obtained from linear interpolation.

Baseflow recession analysis. Recession curves have been analysed for time-series of at least 60 days, where daily rainfall is below potential evapotranspiration and cumulated rainfall <25 mm for each recession curve. The first 15 days of each recession are not considered when fitting the recession model. Both linear and nonlinear models are fitted to the relationship between river discharge Q and storage S: $Q = aS^b$. Analytically, exponent b changes from 1 when transmissivity is constant over time (most likely for confined or very deep unconfined aquifers) to 2 for unconfined flow[21]. Coefficient a is the inverse of the response time when $b \sim 1$.

The annual snow and glacier melt contribution is estimated from the baseflow offset between glaciated and unglaciated basins along the discharge axis of the hysteresis plots (Fig. 2b). The scatter of baseflow within unglaciated basins (~5 mm/month) is considered as uncertainty. For the Mount Everest region (here, Dudh Koshi, station 670), our estimated melt volume ($0.6\,km^3\,yr^{-1}$, Table 1) is consistent with independent glacier mass-loss estimates, measured on ~10% of the glaciated area using satellite altimetry[27].

Hydrological modelling. We consider parsimonious conceptual models at daily and monthly timescales, GR4J and GR2M (http://www.cemagref.fr/webgr/IndexGB.htm). The initial versions have been built up on four and two parameters respectively. We added a distributed snow module based on the HBV conceptual approach[20]. Data scarcity and the requirement of a parsimonious model structure prevented application of a more complex approach. Rainfall and temperature data are redistributed on the ETOPO2v2 (2″ resolution) elevation grid. The parameter Tsep separates rainfall and snowfall (Supplementary Fig. S3). The fusion temperature (T_f) is set to 0 °C. Snow melt (S_m) is driven by a degree-day approach with a constant melting factor M, $S_m = M(T - T_f)$. The snow module adds two parameters to the initial GR2M and GR4J models for the whole basin. Modelled snow cover fractions are validated on MODIS snow cover[25] extent ($r^2 = 0.8$).

The modified GR2M is based on three storage compartments; the snow storage, soil store and routing store, interpreted as 'groundwater storage' (Supplementary Fig. S3). Liquid rainfall and snow melt are partitioned into excess rainfall, actual evapotranspiration, slow percolation and water remaining in the soil store based on a single parameter. Actual evaporotranspiration is driven by potential evaporotranspiration and reservoir water availability. At monthly timescales, the routing store gathers all water and computes discharge. The model discharge calculation was modified on a physical basis to include a priori linear behaviour from recession curve analysis with a variable time response X5, $Q = R/X5$. GR models allow water exchanges with outside the basin (for example subsurface flow) computed with the parameter $X2$. A first order estimate of the groundwater flux contribution to river discharge is computed by tracking water flow from the routing store of GR4J model.

Modulation of hysteresis effect. The shape of the hysteresis curve is used to deduce catchment groundwater storage capacity. Forward modelling studies allow stepwise interpretation of the hysteresis shape with respect to hydrological processes or observation errors, which might have the potential to explain the hysteresis effect. The Rapti catchment (station 360 unglaciated, with no snow) is considered as a reference to test the cumulative impact of several contributions.

We tested four factors, the first being the effect of a systematic underestimation of precipitation and snow on the shape of the hysteresis loop. Applying 30% of excess rainfall[10] shrinks the hysteresis along the precipitation axis (Supplementary Fig. S5a). The second was the impact of snow storage and a delayed melting contribution to discharge, using GLDAS-NOAH model output[28] as a realistic a priori estimate ($100\,mm\,snow\,yr^{-1}$). The snow melt contribution drags the baseflow upward (in March, April and June) but does not change the general shape of the hysteresis loop (Supplementary Fig. S5a). The third was the effect of t_c on the shape of hysteresis loops, where the decrease of t_c from ~45 to 10 days and the associated decrease of the storage capacity does not allow the reproduction of the hysteresis loops observed (Supplementary Fig. S5c). The last was the effect of glacier melt on the shape of the hysteresis loops, where we considered a glacier melt contribution at a constant rate and following a seasonal temperature cycle. This induces a year-long vertical shift of the hysteresis curve (increased baseflow), keeping its shape intact (Supplementary Fig. S5b).

Received 15 April 2011; accepted 25 November 2011; published online XX Month XXXX

References

1. Alley, W. M., Healy, R. W., LaBaugh, J. W. & Reilly, T. E. Flow and storage in groundwater systems. *Science* **296,** 1985–1990 (2002).
2. Oki, T. & Kanae, S. Global hydrological cycles and world water resources. *Science* **313,** 1068–1072 (2006).
3. Bookhagen, B. & Burbank, D. W. Toward a complete Himalayan hydrological budget: Spatiotemporal distribution of snowmelt and rainfall and their impact on river discharge. *J. Geophys. Res.* **115,** 1–25 (2010).
4. Scherler, D., Bookhagen, B. & Strecker, M. R. Spatially variable response of Himalayan glaciers to climate change affected by debris cover. *Nature Geosci.* **4,** 156–159 (2011).
5. Anderson, S. P., Dietrich, W. E. & Brimhall, G. H. Weathering profiles, mass-balance analysis, and rates of solute loss: Linkages between weathering and erosion in a small, steep catchment. *Geol. Soc. Am. Bull.* **114,** 1143–1158 (2002).
6. Tipper, E. *et al.* The short term climatic sensitivity of carbonate and silicate weathering fluxes: Insight from seasonal variations in river chemistry. *Geochim. Cosmochim. Acta* **70,** 2737–2754 (2006).
7. Calmels, D. *et al.* Contribution of deep groundwater to the weathering budget in a rapidly eroding mountain belt, Taiwan. *Earth Planet. Sci. Lett.* **303,** 48–58 (2011).
8. Montgomery, D. R. & Manga, M. Streamflow and water well responses to earthquakes. *Science* **300,** 2047–2049 (2003).
9. Barros, A. P., Chiao, S., Lang, T. J., Burbank, D. & Putkonen, J. From weather to climate—Seasonal and interannual variability of storms and implications for erosion processes in the Himalaya. *Geol. Soc. Am. Spec. Pap.* **398,** 17–38 (2006).
10. Andermann, C., Bonnet, S. & Gloaguen, R. Evaluation of precipitation data sets along the Himalayan front. *Geochem. Geophys. Geosys.* **12,** Q07023 (2011).
11. Shrestha, M. L. Interannual variation of summer monsoon rainfall over Nepal and its relation to Southern Oscillation Index. *Meteorol. Atmos. Phys.* **75,** 21–28 (2000).
12. Bookhagen, B., Thiede, R. & Strecker, M. Abnormal monsoon years and their control on erosion and sediment flux in the high, arid northwest Himalaya. *Earth Planet. Sci. Let.* **231,** 131–146 (2005).
13. Immerzeel, W., Droogers, P., Dejong, S. & Bierkens, M. Large-scale monitoring of snow cover and runoff simulation in Himalayan river basins using remote sensing. *Remote Sens. Environ.* **113,** 40–49 (2009).
14. Hannah, D., Kansakar, S., Gerrard, A. & Rees, G. Flow regimes of Himalayan rivers of Nepal: Nature and spatial patterns. *J. Hydrol.* **308,** 18–32 (2005).
15. Bookhagen, B. & Burbank, D. W. Topography, relief, and TRMM-derived rainfall variations along the Himalaya. *Geophys. Res. Lett.* **33,** L084505 (2006).
16. Putkonen, J. K. Continuous snow and rain data at 500 to 4400 m altitude near Annapurna, Nepal, 1999–2001. *Arct. Antarct. Alpine Res.* **36,** 244–248 (2004).
17. Lambert, L. & Chitrakar, B. Variation of potential evapotranspiration with elevation in Nepal. *Mountain Res. Dev.* **9,** 145–152 (1989).
18. Mouelhi, S., Michel, C., Perrin, C. & Andreassian, V. Stepwise development of a two-parameter monthly water balance model. *J. Hydrol.* **318,** 200–214 (2006).
19. Wang, Q. J. *et al.* Monthly versus daily water balance models in simulating monthly runoff. *J. Hydrol.* **404,** 166–175 (2011).
20. Bergström, S. in *The HBV Model. Computer Models in Watershed Hydrology* (ed. Singh, V. P.) 443–476 (Water Resources Publ., 1995).
21. Wittenberg, H. Baseflow recession and recharge as nonlinear storage processes. *Hydrol. Process.* **13,** 715–726 (1999).
22. Dongol, B. S. *et al.* Shallow groundwater in a middle mountain catchment of Nepal: Quantity and quality issues. *Environ. Geol.* **49,** 219–229 (2005).
23. De Marsily, G. *Quantitative Hydrogeology: Groundwater Hydrology for Engineering* (Academic, 1986).

24. Yatagai, A. *et al.* A 44-year daily gridded precipitation dataset for Asia based on a dense network of rain gauges. *Sola* **5,** 137–140 (2009).
25. Hall, D. K., Riggs, A. G. & Salomonson, V. V. MODIS/Terra Snow Cover 8-Day L3 Global 0.05deg CMG V005, MOD10C2. National Snow and Ice Data Center. Digital media (2006 updated daily).
26. Mitchell, T. D. & Jones, P. D. An improved method of constructing a database of monthly climate observations and associated high-resolution grids. *Int. J. Clim.* **25,** 693–712 (2005).
27. Bolch, T., Pieczonka, T. & Benn, D. I. Multi-decadal mass loss of glaciers in the Everest area (Nepal Himalaya) derived from stereo imagery. *Cryosphere* **5,** 349–358 (2011).
28. Rodell, M. *et al.* The global land data assimilation system. *Bull. Am. Meteorol. Soc.* **85,** 381–394 (2004).
29. National Snow and Ice Data Center. World glacier inventory. World Glacier Monitoring Service and National Snow and Ice Data Center/World Data Center for Glaciology. Digital media. (1999 updated 2009).
30. Department of Mines and Geology Nepal. Geological Map of Nepal. 1:1.000.000 (1994).

Acknowledgements

C.A. benefited from a three years PhD scholarship awarded by the German Academic Exchange Service (DAAD, D/08/42538) and from the French–German double PhD program of the French–German University Saarbrücken (DFH/UFA). The authors like to thank K. P. Sharma and his team from the Department of Hydrology and Meteorology of Nepal (DHM) for providing hydrological data and M. Dhakal from ICIMOD Nepal for sharing their additional information on dug-well measurements.

Author contributions

C.A. acquired and analysed the data. L.L. and C.A. performed the hydrological modelling. All authors discussed the results and wrote the manuscript.

Additional information

The authors declare no competing financial interests. Supplementary information accompanies this paper on www.nature.com/naturegeoscience. Reprints and permissions information is available online at http://www.nature.com/reprints. Correspondence and requests for materials should be addressed to C.A.